Am J Transl Res 2026;18(8):7259-7270
www.ajtr.org /ISSN:1943-8141/AJTR0173806

Original Article

Explainable machine learning-based multiphase contrast-enhanced CT radiomics for noninvasively predicting GPC3 expression in hepatocellular carcinoma: a bicentric study

Wangwang Lin[1], Changkai Chen[2], Xue Wang[1]

[1]*Department of Radiology, The Second Affiliated Hospital of Wenzhou Medical University, Wenzhou, Zhejiang, China;* [2]*Department of Radiology, The First People's Hospital of Yancheng City, Yancheng, Jiangsu, China*

Received May 5, 2026; Accepted July 1, 2026; Epub August 15, 2026; Published August 30, 2026

Abstract: Objectives: Accurate pre-operative prediction of Glypican-3 (GPC3) profiles in hepatocellular carcinoma (HCC) is essential for selecting candidates for targeted therapy and individualized treatment. This study aimed to develop and externally validate an explainable machine learning model for noninvasively prediction of GPC3 expression in HCC. Methods: A total of 301 HCC patients were retrospectively enrolled from two centers (Center 1: 241; Center 2: 60) between January 2016 and September 2024. Radiomics features were extracted from arterial (AP), portal venous (PVP), and delayed phase (DP) images. Robust features were selected via a sequential pipeline including interobserver agreement screening (intraclass correlation coefficient [ICC] > 0.8), Spearman correlation analysis (P > 0.85), and recursive feature elimination (RFE). Single-phase (AP, PVP, DP), combined-phase (APD) radiomics, clinical, and clinical-radiomics models were constructed. Model performance was evaluated using the area under the receiver operating characteristic curve (AUC), and SHAP analysis was applied for model interpretability. Results: The combined clinical-radiomics model outperformed the clinical model, achieving an AUC of 0.886 in the training cohort, 0.880 during internal validation cohort, and 0.839 during external validation cohort (P < 0.05). The APD radiomics model showed performance non-inferior to that of the combined model (P > 0.05) and outperformed all single-phase models. AFP > 7 ng/mL (OR=3.257) and intratumoral necrosis (OR=2.947), as confirmed by multivariate logistic regression, were independent predictors for GPC3 positivity. SHAP analysis further identified radiomics score as the most influential predictor (mean |SHAP|=1.84). Conclusion: The multiphase CECT radiomics-based combined model demonstrates good cross-center generalizability and enables accurate noninvasive prediction of GPC3 expression status in HCC. This model may provide a reliable imaging-based tool for screening candidate patients for GPC3-targeted therapies.

Keywords: Hepatocellular carcinoma, glypican-3, radiomics, machine learning, tomography, X-ray computed, multiphase

Introduction

Globally, hepatocellular carcinoma (HCC) ranks among the most prevalent liver malignancies. Despite continuous advances in diagnostic and therapeutic strategies, its insidious onset and rapid progression have led to a persistent increase in both incidence and mortality rates [1]. Moreover, HCC is highly and biologically heterogeneous, as its histopathological manifestations and molecular expression profiles change depending on etiological factors. Hence, disease progression, therapeutic response, and clinical outcomes differ substantially among individuals, posing significant challenge to precise HCC diagnosis and management [2, 3]. Thus, in-depth investigation of HCC etiology and pathogenesis, and elucidation of its molecular features, remains essential for advancing personalized treatment and improving clinical outcome.

Glypican-3 (GPC3), a heparan sulfate proteoglycan family member, is anchored to the extracellular surface of the cell membrane via a glycosylphosphatidylinositol (GPI) linkage. Regarding

https://doi.org/10.62347/IVMH4590

its expression patterns, GPC3 exhibits a clear tumor-selective nature, with markedly upregulated protein abundance in HCC tissue, while being absent of expressed at very low levels in normal adult hepatocytes and benign hepatic lesions [4]. Accumulating evidence has demonstrated that GPC-3 positivity is associated with increased tumor invasiveness, higher recurrence risk, and poorer survival outcomes in HCC patients [5-7]. By modulating multiple signaling pathways and thereby influencing tumor cell behaviors (e.g., proliferation, differentiation, invasion, and migration), GPC-3 plays a critical role in the pathogenesis and malignant progression of HCC [8]. Besides, its cell surface and relatively low off-target expression in normal tissues make GPC3 an ideal target for targeted therapy and immunotherapy [9]. Accordingly, accurate assessment GPC3 expression in HCC is of significant implications for identifying suitable candidates for targeted therapy and optimizing individualized treatment strategies.

Currently, GPC3 quantification mainly relies on serological assays and immunohistochemistry. Although GPC3 can be detected in peripheral circulations after shedding from tumor cell membranes, serological testing is limited in clinical utility due to its relatively low specificity and sensitivity [6, 10]. Immunohistochemistry remains the "gold standard" for GPC3 assessment; however, it is invasive and associated with sampling bias and potential risks such as bleeding or tumor dissemination. Moreover, it fails to adequately capture intratumoral spatial heterogeneity [6, 11]. Therefore, it is of great significance to develop a noninvasive, quantitative, and reproducible preoperative approach for accurate prediction of GPC3 expression in HCC.

Imaging plays an important supplementary role in molecular and pathological assessments. It offers distinct advantages, including convenient, cost-effectiveness, and noninvasiveness, making it a preferred modality for evaluating HCC biology, progression, and prognosis [12]. Multiphase contrast-enhanced computed tomography (CECT) and dynamic contrast-enhanced magnetic resonance imaging (DCE-MRI) are commonly used imaging techniques if HCC diagnosis. They can noninvasively and clearly display tumor size, morphological characteristics, perfusion patterns, and depth of invasion. Imaging features such as tumor margins, enhancement patterns, and intratumoral necrosis (ITN), have been identified by radiologists as having potential value in assessing HCC aggressiveness and predicting prognosis. However, as these evaluations are largely experience-dependent, and issues such as inter-observer variability and the lack of standardized assessment cause significant limitations [13].

Radiomics is an emerging imaging analysis technique. By using algorithms to extract high-throughput two- and higher-dimensional features from medical images, radiomics enables objective characterization of intratumoral microstructural heterogeneity. When combined with machine learning (ML) algorithms, it substantially expands the utility of medical imaging by linking imaging phenotypes with tumor molecular characteristics and clinical outcomes [14]. Compared to conventional subjective visual assessment, radiomics is computationally stable, highly reproducible, and less subjective to observer bias, and has been widely applied in HCC diagnosis, relapse prediction, efficacy evaluation, and risk stratification [15]. In HCC, MRI-based radiomics has also shown promise in predicting GPC3 expression [16-18].

However, existing studies still have two major shortcomings. First, most current radiomics models for predicting GPC3 expression still lack sufficient interpretability. Although they often achieve high predictive performance, they provide limited insight into which imaging features drive model decisions or how these features reflect underlying tumor spatial heterogeneity. This lack of biological and imaging interpretability limits clinicians' understanding and confidence in model predictions, thereby hindering clinical translation. Second, CT-based evidence for GPC3 prediction remains relatively limited. Compared to MRI, CT offers advantages such as wider accessibility, shorter acquisition times, lower costs, and higher inter-institutional standardization. However, most CT radiomics studies are still confined to single-center cohorts and lack external validation, limiting their generalizability and clinical applicability.

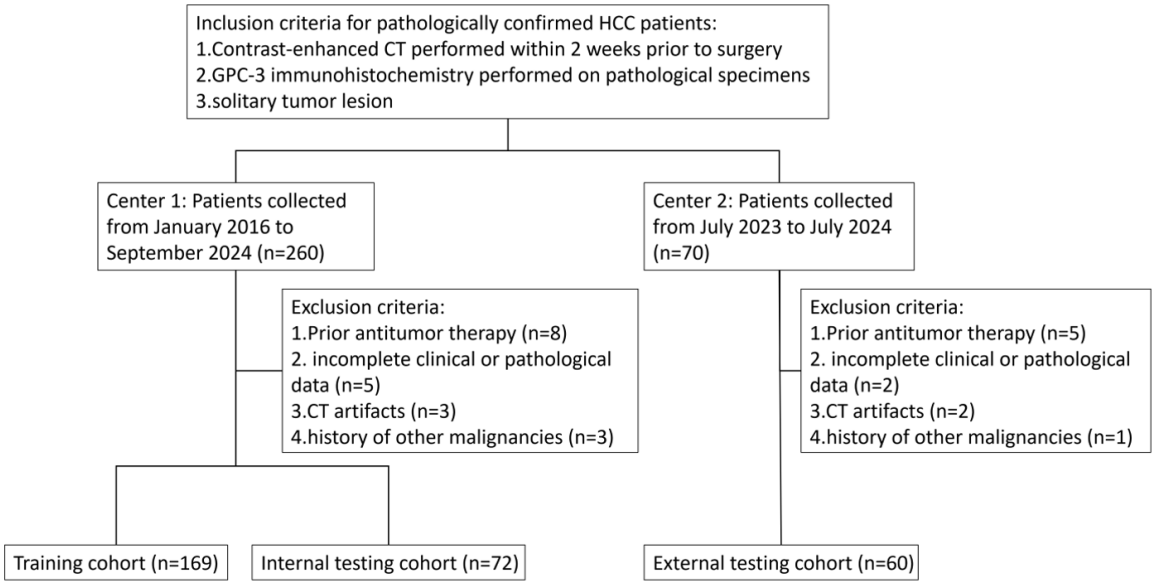

Figure 1. Flowchart of study population selection.

To address these key limitations, we propose an interpretable machine learning framework based on a retrospective, two-center cohort. Unlike previous single-phase or single-center designs, we systematically extracted and integrated radiomic features from three consecutive CTEC phases (arterial, portal, and delayed phases) to comprehensively capture spatiotemporal heterogeneity of tumor perfusion in GPC3-positive HCC. Crucially, SHapley Additive exPlanations (SHAP) was applied to quantify and visualize feature contributions, thereby improving model interpretability. The aim is to render a noninvasive, accurate GPC3 prediction tool to assist in tailored HCC treatment.

Materials and methods

Study design and patients

This retrospective, multicenter study was approved by the institutional review boards of The Second Affiliated Hospital of Wenzhou Medical University and The First People's Hospital of Yancheng City. The requirement for informed consent was waived due to the retrospective nature of the study.

Data were collected from surgically treated HCC patients at two centers: The Second Affiliated Hospital of Wenzhou Medical University (Center 1; January 2016-September 2024), and The First People's Hospital of Yancheng City (Center 2; July 2023-July 2024). Inclusion criteria: (1) CECT performed within 2 weeks prior to surgery, with adequate image quality; (2) postoperative histopathological confirmation of HCC with GPC3 expression assessed by immunohistochemistry; (3) solitary HCC lesion without multi-focal cancers; (4) availability of complete clinical, pathological, and imaging data. Exclusion criteria: (1) prior anti-tumor treatments (e.g., chemotherapy, radiotherapy, targeted therapy, or immunotherapy); (2) incomplete clinical/pathological data; (3) difficulty to clearly delineate lesions due to CT artifacts; or (4) a history of other malignancies.

Following rigorous screening, 301 patients were included, comprising 241 cases from Center 1 and 60 from Center 2. Patients from Center 1 were randomly allocated to a training cohort (n=169) and an internal validation cohort (n=72), at a 7:3 ratio. Patients from Center 2 (n=60) served as an independent external validation cohort to evaluate model generalizability (**Figure 1**).

CT imaging protocol

All cases received a triphasic contrast-enhanced liver scan using a multi-detector spiral CT scanner (Philips Brilliance iCT, GE Optima CT660, or Siemens Somatom Force). Scanning parameters included: detector collimation of 128×0.625 mm, 64×0.625 mm, or 192×0.6 mm; field of view, 30-38 cm; pitch, 0.8-1.0;

matrix, 512×512; tube voltage, 100-120 kV; tube current, 250-350 mA; and reconstructed slice thickness/increment of 1 mm. Routine diagnostic images were reconstructed at a 5-mm slice thickness. All patients were scanned in the supine position and instructed to hold their breath during acquisition.

Iopromide (Ultravist 300, Bayer Schering Pharma, Germany) was administered at a dose of 1.5 ml/kg via an antecubital vein at an injection rate of 3-4 ml/s using a power injector (Ulrich CT Plus 150). A bolus tracking technique was used to initiate scanning automatically. Images were acquired during the arterial phase (AP; 25-35s post-injection), portal venous phase (PVP; 60-70s post-injection), and delayed phase (DP; 180-240s post-injection) after contrast injection, and subsequently transferred to the Picture Archiving and Communication System (PACS) for further analysis.

Clinical and CT imaging feature collection

Clinical, preoperative laboratory, and postoperative pathological information were retrieved from electronic medical records, including age, sex, hepatitis B virus infection status, alpha-fetoprotein (AFP) level, and other serum markers. Two abdominal radiologists (with 3 and 5 years of experience, respectively), who were blinded to pathological and clinical outcomes, independently reviewed CT images. Imaging features included tumor size, tumor margin, enhancement pattern, capsule enhancement, ITN, peritumoral arterial phase hyperenhancement, intralesional vessels, and presence of intralesional fat or hemorrhage. Discrepancies were resolved through consensus discussion.

Histopathological analysis

Following fixation in 10% neutral buffered formalin and paraffin-embedding, surgical specimens were prepared into 4-μm thick sections. GPC3 expression was detected using the streptavidin-peroxidase (SP) immunohistochemical method. According to established criteria [19], GPC3 positivity was defined as immunoreactivity in ≥ 5% of tumor cells, whereas < 5% or no staining was considered negative. Histopathological evaluation was independently performed by two experienced pathologists (each > 5 years of experience in hepatobiliary pathology), and any disagreements were resolved by consensus.

Radiomics workflow

Region of interest (ROI) segmentation: Image segmentation was performed on AP, PVP, and DP images of HCC patients. Two radiologists independently performed 3D segmentation using 3D Slicer software (version 5.6.2), and both were blinded to the pathological results. A semi-automatic segmentation tool was applied. Radiologist 1 delineated the volume of interest (VOI) along the tumor margins and, when necessary, manually refined the segmentation on a slice-by-slice basis to exclude necrotic/cystic areas (CT value < 20 HU), large vessels (diameter > 3 mm), and adjacent normal liver tissues, ensuring a full coverage of the viable tumor region. Physician 2 performed independent VOI segmentation using the same protocol. Inter-observer consistency was assessed using the intraclass correlation coefficient (ICC).

Radiomics feature extraction and selection: Radiomics features of the VOIs were extracted using PyRadiomics (version 3.1.0). To reduce heterogeneity introduced by different CT scanners and acquisition parameters, all images underwent standardized resampling, with isotropic voxel spacing of 1×1×1 mm^3. Meanwhile, a fixed bin width (25 HU) was used to complete the voxel intensity quantification processing. Shape-based, first-order statistical, texture (e.g., GLCM, GLRLM), and wavelet-transformed features were extracted, with 2,154 features per phase retained after applying wavelet and Laplacian of Gaussian filters.

To minimize redundancy and prevent model overfitting, feature selection was performed in four steps: (1) Reproducibility filtering: Only features with ICC > 0.8 were retained. (2) Standardization: retained features were standardized using Z-score transformation. (3) Redundancy reduction: Spearman correlation analysis was performed, and for feature pairs with $|P| > 0.85$, one was removed. (4) Feature optimization: recursive feature elimination (RFE) with logistic regression (LR) was used to select the top 20 features associated with GPC3 expression (**Figure 2**).

Model development and validation

Univariate LR analysis was performed to identify GPC3 expression-associated clinical and CT imaging features ($P < 0.05$). Variables showing statistical significance were subsequently

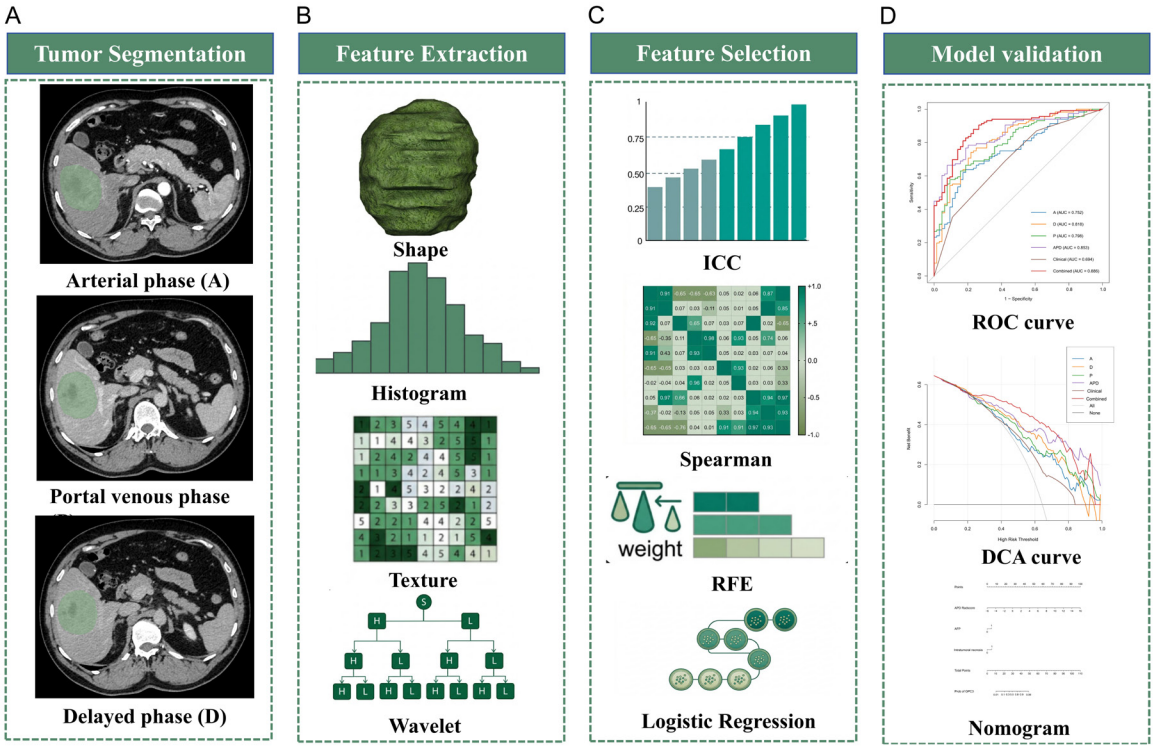

Figure 2. Radiomics workflow. The workflow includes: (A) tumor segmentation on multiphase CT images, (B) extraction of radiomics features, including morphology, histogram, texture, and wavelet features; (C) feature selection using ICC, Spearman correlation, and RFE; (D) model development and validation using ROC curves, DCA, and nomograms. Notes: ICC, intraclass correlation coefficient; RFE, recursive feature elimination; ROC, receiver operator characteristic curve; DCA, decision curve analysis.

entered into a multivariate LR model to determine independent predictors.

A radiomics score (Rad-score) was constructed for each imaging phases (AP, PVP, DP) as well as the combined multiphase model (APD) by linearly weighting the selected radiomics features according to their LR coefficients. Six predictive models were then developed: (1) Clinical Model (independent clinical risk factors only); (2) AP Radiomics Model (AP-Rad-score only); (3) PVP Radiomics Model (PVP-Rad-score only); (4) DP Radiomics Model (DP-Rad-score only); (5) APD Radiomics Model (APD-Rad-score only); and (6) Combined Model (independent predictors + APD-Rad-score).

All models were built using the scikit-learn library (version 1.8.0). Hyperparameter optimization was performed using randomized search with 10-fold cross-validation in the training set. Model performance was evaluated using the AUC, sensitivity, and specificity, reported with 95% confidence intervals (CIs). A nomogram was subsequently developed based on the combined model.

Statistical analysis

Statistical analyses were processed using SPSS (version 31.0) and R software (version 4.4.1). Data normality was tested using the Shapiro-Wilk test. Continuous variables were compared using the independent samples t-test for normally distributed data and the Mann-Whitney U test for non-normally distributed data. Categorical data were analyzed using the chi-square test or Fisher's exact test, as appropriate. The DeLong test was used to compare the AUCs of different models. Calibration curves were generated to evaluate the agreement between observed and estimated probabilities, and decision curve analysis (DCA) evaluated the model's clinical utility.

Model interpretability

Model interpretability was assessed using SHAP. SHAP values were calculated for each feature, enabling both local and global interpretation of model outputs. This approach improved transparency by illustrating how each variable influenced the final prediction of GPC3 expression.

Results

Patient features

Among the 301 HCC cases selected (244 male, 81.1%), GPC3 positivity was confirmed in 193 (64.1%) by postoperative pathological examination. There were no significant differences in baseline clinical, laboratory, or CT imaging characteristics among the training, internal validation, and external validation cohorts (all $P > 0.05$), indicating well-balanced datasets suitable for model development and validation (**Table 1**).

Univariate logistic regression analysis showed that GPC3 positivity was associated with AFP > 7 ng/mL, ITN, and capsular enhancement ($P < 0.05$). In multivariate analysis, AFP > 7 ng/mL (OR=3.257, 95% CI: 1.671-6.348, P=0.001) and ITN (OR=2.947, 95% CI: 1.480-5.870, P=0.002) were identified as independent predictors of GPC3 positivity (**Table 2**).

Radiomics feature selection

From the 2,154 radiomics features extracted per imaging phase, 1,120 (AP), 981 (PVP), and 1,046 (DP) features with high reproducibility (ICC > 0.8) were retained. Subsequently, Spearman correlation analysis and recursive feature elimination (RFE) were applied, resulting in the selection of the top 20 most informative features for each model.

Model performance

The performance of all models is summarized in **Table 3**. The combined model demonstrated the best predictive performance, with AUCs of 0.886 in the training cohort, 0.880 in the internal validation cohort, and 0.839 during the external validation cohort, outperforming the clinical model ($P < 0.05$).

The APD radiomics model and the combined model demonstrated equivalent performance ($P > 0.05$), superior to all single-phase models. The clinical model showed the poorest performance across all cohorts. **Figure 3** displays the nomogram, ROC curves, DCA, and calibration curves for the external validation cohort. DCA demonstrated that the combined model yielded the highest net benefit across a wide range of threshold probabilities. Calibration curves indicated good agreement between predicted and actual GPC3 status.

Model interpretability

SHAP was performed to interpret model decision-making and quantify feature contributions. The APD-Rad-score was the most critical predictor (average |SHAP|=1.84). Higher Rad-score values were associated with an increased probability of GPC-3 positivity predicted by the model. ITN (average |SHAP|=0.48) and AFP (average |SHAP|=0.44) also positively contributed to model predictions. However, their contributions were substantially lower than those of the APD Rad-score, indicating that radiomics features played a dominant role in model decision-making (**Figure 4**).

Discussion

In this study, we developed and validated a multiphase CECT radiomics-based machine learning model for noninvasive GPC3 predictions in HCC. The combined model (radiomics + clinical features) achieved the best performance (training AUC=0.886, internal validation AUC=0.880, and external validation AUC=0.839), outperforming the clinical-only model. Furthermore, the APD radiomics model showed non-inferior performance compared with the combined model and outperformed all single-phase models, suggesting that integration of multiphase imaging information is essential for capturing tumor biological heterogeneity.

With the rapid development of technology, MRI-based radiomics has been widely applied in studies of GPC-3 prediction and has achieved remarkable diagnostic performance. For example, a multi-sequence MRI-based radiomics nomogram demonstrated excellent predictive accuracy (training AUC=0.985, validation AUC=0.989) [17]. However, CT remains more widely

Table 1. Clinical and imaging features of included patients

Characteristic	Training cohort (N=169)				Internal Test Cohort (N=72)				External Test Cohort (N=60)			
	GPC3 (+) (n=109)	GPC3 (-) (n=60)	χ^2/t	*P*-value	GPC3 (+) (n=46)	GPC3 (-) (n=26)	χ^2/t	*P*-value	GPC3 (+) (n=38)	GPC3 (-) (n=22)	χ^2/t	*P*-value
Age (years, mean ± SD)	53.53±9.79	52.75±10.63	0.481	0.632	50.53±9.28	49.96±9.56	0.248	0.705	51.65±8.93	48.60±8.49	1.298	0.199
Gender, n (%)			0.528	0.468			0.124	0.725			0.643	0.423
Male	92 (84.4)	48 (80.0)			37 (80.4)	20 (76.9)			31 (81.6)	16 (72.7)		
AFP > 7 ng/mL, n (%)	67 (61.5)	38 (63.3)	0.027	0.811	26 (72.2)	13 (52.0)	0.285	0.594	24 (63.2)	13 (59.1)	0.097	0.755
Intratumoral necrosis, n (%)	39 (36.1)	20 (33.3)	0.102	0.750	14 (30.4)	9 (34.6)	0.134	0.715	17 (44.7)	8 (36.4)	0.402	0.526
Tumor size (mm, mean ± SD)	48.19±36.03	49.28±31.39	0.197	0.844	43.78±24.39	56.24±34.76	1.780	0.079	46.52±33.65	53.28±38.77	0.709	0.481

Note: Only key differentiating and demographic features are shown for brevity. Full table available in source document. AFP, alpha-fetoprotein.

Table 2. Univariate and multivariate logistic regression analyses of clinical and imaging factors associated with GPC3 expression in HCC

Variable	Univariate Analysis		Multivariate Analysis	
	OR (95% CI)	*P*-value	OR (95% CI)	*P*-value
AFP > 7 ng/mL	1.917 (1.085-3.388)	0.025	3.257 (1.671-6.348)	0.001
Intratumoral necrosis	2.044 (1.150-3.632)	0.015	2.947 (1.480-5.870)	0.002
Enhancing capsule	0.489 (0.260-0.919)	0.026	0.512 (0.261-1.004)	0.051

Note: AFP, alpha-fetoprotein; OR, odds ratio.

Table 3. Comparison of the predictive performance of each model

Cohort	Model	AUC (95% CI)	Accuracy	Sensitivity	Specificity	*P*-value vs Combined
Training cohort	AP	0.752 (0.681-0.823)	0.700	0.639	0.813	< 0.001
	PVP	0.798 (0.733-0.862)	0.750	0.879	0.516	0.006
	DP	0.818 (0.753-0.883)	0.772	0.888	0.563	0.058
	APD	0.853 (0.799-0.907)	0.789	0.784	0.797	0.050
	Clinical	0.694 (0.614-0.774)	0.650	0.689	0.578	< 0.001
	Combined	0.886 (0.837-0.936)	0.839	0.879	0.766	Ref
Internal Test Cohort	AP	0.710 (0.580-0.840)	0.689	0.889	0.400	0.013
	PVP	0.778 (0.661-0.895)	0.737	0.639	0.880	0.079
	DP	0.710 (0.580-0.840)	0.705	0.750	0.640	0.014
	APD	0.826 (0.724-0.927)	0.750	0.700	0.800	0.144
	Clinical	0.701 (0.568-0.834)	0.639	0.500	0.840	0.004
	Combined	0.880 (0.795-0.965)	0.836	0.778	0.920	Ref
External Test Cohort	AP	0.725 (0.591-0.859)	0.738	0.700	0.800	0.078
	PVP	0.747 (0.615-0.879)	0.769	0.825	0.680	0.181
	DP	0.705 (0.578-0.832)	0.692	0.900	0.360	0.045
	APD	0.810 (0.695-0.925)	0.800	0.850	0.720	0.296
	Clinical	0.700 (0.574-0.825)	0.631	0.550	0.760	0.020
	Combined	0.839 (0.729-0.949)	0.831	0.875	0.760	Ref

Note: AP, arterial phase; PVP, portal venous phase; DP, delayed phase; APD, combined-phase.

used in clinical practice due to its higher accessibility, shorter acquisition time, and lower costs. Although our CT-based radiomics model demonstrated a marginally reduced AUC than the aforementioned MRI study, it shows good generalizability (AUC=0.839 in the external validation set). Moreover, a recent study emphasized the importance of intratumoral heterogeneity for GPC3 prediction, reporting AUCs of 0.912 and 0.927 using combined habitat and peritumoral radiomics approaches [20]. In contrast, our study, through AP, PVP, and DP feature fusion, captures time-dependent hemodynamic heterogeneity of the tumor. Both methodological approaches confirm the feasibility and clinical potential of CT radiomics for noninvasive prediction of GPC3 expression.

Multiphase CT feature fusion plays a central role in improving model performance. Previous studies on multiphase CT radiomics for liver cancers showed that AP (displaying tumor blood supply), PVP (reflecting portal perfusion), and DP (indicating contrast washout) provide distinct information that depicts the whole picture of tumor biology [21]. Echoing past literature [22], our results also showed that the APD radiomics model outperformed single-phase models. SHAP analysis further revealed that the APD Rad-score was the most significant contributor, with substantially greater contribution than clinical variables such as AFP and ITN. These findings suggest that multiphase radiomics effectively quantifies tumor microenvironment heterogeneity associated with GPC-3 expression and plays a dominant role in model prediction.

AFP > 7 ng/mL was identified by multivariate logistic regression analysis as an independent determinant for differentiating GPC3-positive and GPC3-negative HCC, which is consistent with previously reported associations between AFP and GPC3 expression in HCC carcinogenesis [10]. Biologically, both AFP and GPC3 are oncofetal proteins that are highly expressed during embryonic development but are largely silenced in normal adult tissues. They may synergistically participate in hepatocarcinogenesis by modulating key oncogenic signaling pathways, including Wnt/β-catenin and PI3K/Akt/mTOR pathways, thereby promoting tumor cell proliferation, invasion, and metastasis [5]. However, AFP alone is insufficient for accurate prediction of GPC3 expression. This is justified by the observation that approximately 30-40% of HCC cases present with normal AFP levels despite potentially high GPC3 levels [10]. In

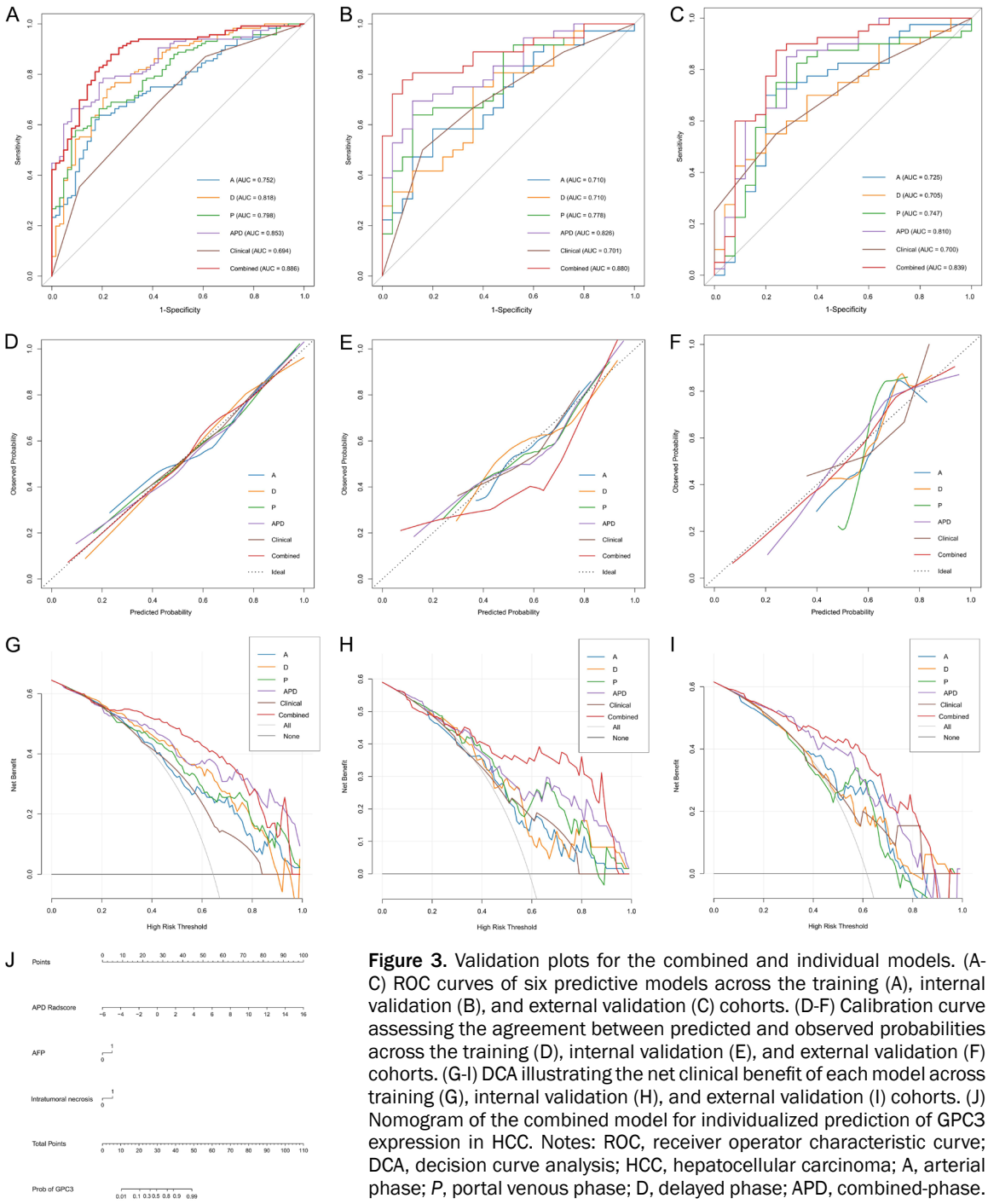

Figure 3. Validation plots for the combined and individual models. (A-C) ROC curves of six predictive models across the training (A), internal validation (B), and external validation (C) cohorts. (D-F) Calibration curve assessing the agreement between predicted and observed probabilities across the training (D), internal validation (E), and external validation (F) cohorts. (G-I) DCA illustrating the net clinical benefit of each model across training (G), internal validation (H), and external validation (I) cohorts. (J) Nomogram of the combined model for individualized prediction of GPC3 expression in HCC. Notes: ROC, receiver operator characteristic curve; DCA, decision curve analysis; HCC, hepatocellular carcinoma; A, arterial phase; *P*, portal venous phase; D, delayed phase; APD, combined-phase.

contrast, our combined model integrates clinical biomarkers with radiomics features, thereby incorporating both tumor microstructural heterogeneity and perfusion characteristics to overcome the limitations of single biomarkers.

ITN, another identified independent predictor, is also of important clinical relevance [23]. ITN typically manifests as low-attenuation areas on CT imaging, which are mainly attributed to rapid tumor proliferation outpacing vascular supply, leading to hypoxia in the tumor microenvironment. This imaging feature may reflect hypoxia-inducible factor (HIF) activation, which mediates GPC3 upregulation via the Wnt/β-catenin axis [16, 24]. In HCC lesions exhibiting ITN on

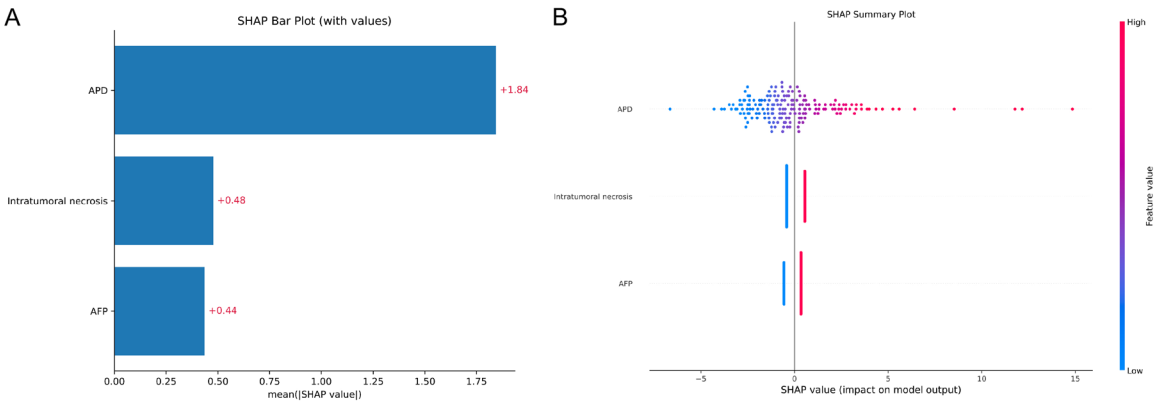

Figure 4. SHAP analysis of the combined model. A. SHAP bar plot displaying the mean absolute SHAP values of the top three features, indicating their overall contribution to model prediction. B. SHAP summary plot illustrating each feature's influence on model outputs. Each point represents a single patient. Different colors are used to distinguish the differences in feature value: red indicates a high feature value, while blue indicates a low feature value. The X-axis values represent the SHAP values, which are used to quantify each factor's impact on the predicted outcome. Notes: AFP, alpha-fetoprotein; APD, combined-phase; SHAP, SHapley additive explanation.

CT, the corresponding pathological tissue often demonstrates high proliferative activity and aggressive invasion, consistent with a GPC3-high expression phenotype [12, 25]. The incorporation of radiomics features in our combined model, which effectively captured ITN-associated imaging heterogeneity, likely contributed to its superior predictive performance.

Several limitations of this study should be acknowledged. First, the retrospective design inherently introduces potential selection bias, necessitating future prospective multicenter studies for further validation. Second, despite bicentric sample collection, the overall sample size remains relatively limited. In particular, the sample size in the external validation cohort was small, which may have contributed to the widening of the 95% CIs and the observed decrease in AUC from 0.886 to 0.839. In radiomics studies, such performance observed is typically attributed to batch effects arising from differences in scanner manufacturers, imaging acquisition parameters, and regional patient heterogeneity. Nevertheless, an external validation AUC of 0.839 still represents robust and clinically meaningful predictive performance. Third, this study is based solely on CT radiomics. The integration of additional imaging modalities, such as MRI- or PET-CT-based radiomics, may further enhance predictive performance. Furthermore, this study lacks direct biological validation using omics data (e.g., transcriptomic or proteomics), making it difficult to establish a direct mechanistic link between radiomics features and the underlying molecular biology of GPC3 expression. Therefore, future prospective studies incorporating larger, nationwide, and more ethnically diverse multicenter cohorts are warranted. In addition, the application of spatial transcriptomics and radiogenomics/radioproteomics approaches may help bridge the gap between macroscopic imaging phenotypes and microscopic molecular processes underlying GPC3 expression.

Conclusion

The multiphase CECT radiomics-based machine learning model enables noninvasive and accurate prediction of GPC3 expression in HCC. It provides a reliable imaging-based tool for identifying candidates suitable for GPC3-targeted treatment and supports individualized treatment planning, thereby offering important clinical value and translational potential.

Acknowledgements

This project was subsidized by the Wenzhou Basic Public Welfare Scientific Research Project (No. Y2023539).

Disclosure of conflict of interest

None.

Address correspondence to: Xue Wang, Department of Radiology, The Second Affiliated Hospital of Wenzhou Medical University, No. 109 Xueyuan

West Road, Lucheng District, Wenzhou 325027, Zhejiang, China. Tel: +86-0577-88002874; E-mail: wangxue890@foxmail.com

References

[1] Rumgay H, Arnold M, Ferlay J, Lesi O, Cabasag CJ, Vignat J, Laversanne M, McGlynn KA and Soerjomataram I. Global burden of primary liver cancer in 2020 and predictions to 2040. J Hepatol 2022; 77: 1598-1606.

[2] Safri F, Nguyen R, Zerehpooshnesfchi S, George J and Qiao L. Heterogeneity of hepatocellular carcinoma: from mechanisms to clinical implications. Cancer Gene Ther 2024; 31: 1105-1112.

[3] Yang X, Yang C, Zhang S, Geng H, Zhu AX, Bernards R, Qin W, Fan J, Wang C and Gao Q. Precision treatment in advanced hepatocellular carcinoma. Cancer Cell 2024; 42: 180-197.

[4] Schepers EJ, Glaser K, Zwolshen HM, Hartman SJ and Bondoc AJ. Structural and functional impact of posttranslational modification of glypican-3 on liver carcinogenesis. Cancer Res 2023; 83: 1933-1940.

[5] Zhou F, Shang W, Yu X and Tian J. Glypican-3: a promising biomarker for hepatocellular carcinoma diagnosis and treatment. Med Res Rev 2018; 38: 741-767.

[6] Haruyama Y and Kataoka H. Glypican-3 is a prognostic factor and an immunotherapeutic target in hepatocellular carcinoma. World J Gastroenterol 2016; 22: 275-283.

[7] Xiao WK, Qi CY, Chen D, Li SQ, Fu SJ, Peng BG and Liang LJ. Prognostic significance of glypican-3 in hepatocellular carcinoma: a meta-analysis. BMC Cancer 2014; 14: 104.

[8] Li N, Gao W, Zhang YF and Ho M. Glypicans as cancer therapeutic targets. Trends Cancer 2018; 4: 741-754.

[9] Couzinet A, Suzuki T and Nakatsura T. Progress and challenges in glypican-3 targeting for hepatocellular carcinoma therapy. Expert Opin Ther Targets 2024; 28: 895-909.

[10] Xu J, Tan L, Jiang N, Zhang F, Wang J, Li F, Wang J, Li H, Chen L, Mezzetti O, Lin W, Li S and Gao Y. Integrating GPC3 with other biomarkers to improve the diagnosis of early-stage liver cancer. Pathogens 2025; 14: 1189.

[11] Russo FP, Imondi A, Lynch EN and Farinati F. When and how should we perform a biopsy for HCC in patients with liver cirrhosis in 2018? A review. Dig Liver Dis 2018; 50: 640-646.

[12] Jia X, Jiang H, Ye Z, Wei H, Chen J, Qu Y, Sirlin CB, Song B and Wang Y. Imaging for molecular and pathological subtyping of hepatocellular carcinoma-a critical appraisal and future directions. Eur Radiol 2026; 36: 2744-2763.

[13] Ronot M, Chernyak V, Burgoyne A, Chang J, Jiang H, Bashir M and Fowler KJ. Imaging to predict prognosis in hepatocellular carcinoma: current and future perspectives. Radiology 2023; 307: e221429.

[14] Su GH, Xiao Y, You C, Zheng RC, Zhao S, Sun SY, Zhou JY, Lin LY, Wang H, Shao ZM, Gu YJ and Jiang YZ. Radiogenomic-based multiomic analysis reveals imaging intratumor heterogeneity phenotypes and therapeutic targets. Sci Adv 2023; 9: eadf0837.

[15] Harding-Theobald E, Louissaint J, Maraj B, Cuaresma E, Townsend W, Mendiratta-Lala M, Singal AG, Su GL, Lok AS and Parikh ND. Systematic review: radiomics for the diagnosis and prognosis of hepatocellular carcinoma. Aliment Pharmacol Ther 2021; 54: 890-901.

[16] Gao Y, Liu D, Miao Y, Lou Z, Luo Z, Li Y, Cai H, Zhu Y and Chen S. Radiogenomic MRI biomarkers for noninvasive prediction of GPC3 expression and tumor microenvironment in hepatocellular carcinoma. J Transl Med 2025; 24: 198.

[17] Li SQ, Yang CX, Wu CM, Cui JJ, Wang JN and Yin XP. Prediction of glypican-3 expression in hepatocellular carcinoma using multisequence magnetic resonance imaging-based histology nomograms. Quant Imaging Med Surg 2024; 14: 4436-4449.

[18] Chong H, Gong Y, Zhang Y, Dai Y, Sheng R and Zeng M. Radiomics on gadoxetate disodium-enhanced MRI: non-invasively identifying glypican 3-positive hepatocellular carcinoma and postoperative recurrence. Acad Radiol 2023; 30: 49-63.

[19] Takai H, Kato A, Ishiguro T, Kinoshita Y, Karasawa Y, Otani Y, Sugimoto M, Suzuki M and Kataoka H. Optimization of tissue processing for immunohistochemistry for the detection of human glypican-3. Acta Histochem 2010; 112: 240-250.

[20] Zhang J, Zhu X, Qiu J, Shi H, Liu Y, Hua J, Qin X, Dong S, Liu Y, Wu C and Chen J. Noninvasive prediction of Glypican-3 expression in hepatocellular carcinoma using Habitat-based and peritumoral CT radiomics: a nomogram approach. Cancer Imaging 2025; 25: 144.

[21] Tang VH, Duong STM, Nguyen CDT, Huynh TM, Duc VT, Phan C, Le H, Bui T and Truong SQH. Wavelet radiomics features from multiphase CT images for screening hepatocellular carcinoma: analysis and comparison. Sci Rep 2023; 13: 19559.

[22] Wu XA, Su H, Hua Y, Xu Y, Wang L, Wang X, Wang S, Jin B, Liu X, Wan X, Sun Q, Wang X and Du S. A multi-phase CT dataset for automated differential diagnosis of liver tumors. Sci Data 2025; 13: 31.

[23] Zhu L, Li N, Liang S, Jiang B, Li M, Luo Y and Fei X. High frame rate contrast-enhanced ultrasound in hepatocellular carcinoma: biological characteristics and patient outcomes. BMC Cancer 2025; 25: 1488.

[24] Zhang Q, Bai X, Chen W, Ma T, Hu Q, Liang C, Xie S, Chen C, Hu L, Xu S and Liang T. Wnt/β-catenin signaling enhances hypoxia-induced epithelial-mesenchymal transition in hepatocellular carcinoma via crosstalk with hif-1α signaling. Carcinogenesis 2013; 34: 962-973.

[25] Xia TY, Zhou ZH, Meng XP, Zha JH, Yu Q, Wang WL, Song Y, Wang YC, Tang TY, Xu J, Zhang T, Long XY, Liang Y, Xiao WB and Ju SH. Predicting microvascular invasion in hepatocellular carcinoma using CT-based radiomics model. Radiology 2023; 307: e222729.